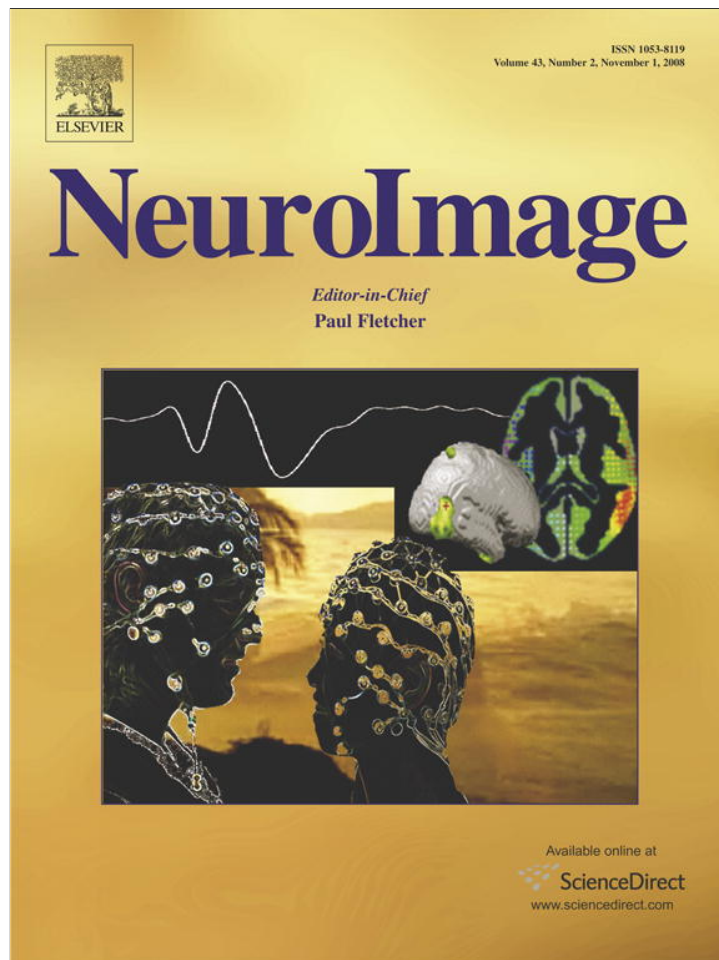


Provided for non-commercial research and education use.
Not for reproduction, distribution or commercial use.



This article appeared in a journal published by Elsevier. The attached copy is furnished to the author for internal non-commercial research and education use, including for instruction at the authors institution and sharing with colleagues.

Other uses, including reproduction and distribution, or selling or licensing copies, or posting to personal, institutional or third party websites are prohibited.

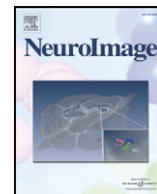
In most cases authors are permitted to post their version of the article (e.g. in Word or Tex form) to their personal website or institutional repository. Authors requiring further information regarding Elsevier's archiving and manuscript policies are encouraged to visit:

<http://www.elsevier.com/copyright>



Contents lists available at ScienceDirect

NeuroImage

journal homepage: www.elsevier.com/locate/ynimg

Use of anisotropic modelling in electrical impedance tomography; Description of method and preliminary assessment of utility in imaging brain function in the adult human head

Juan-Felipe P.J. Abascal^{a,d,*}, Simon R. Arridge^{b,h}, David Atkinson^{d,h}, Raya Horesh^c, Lorenzo Fabrizi^d, Marzia De Lucia^e, Lior Horesh^c, Richard H. Bayford^f, David S. Holder^{d,g}

^a Laboratoire des Signaux et Systèmes, Supélec, Gif-Sur-Yvette, France

^b Department of Computer Science, UCL, London, UK

^c Department of Mathematics and Computer Science, Emory University, Atlanta, GA, USA

^d Department of Medical Physics, UCL, London, UK

^e EEG Brain Mapping Core, Center for Biomedical Imaging of Lausanne and Geneva, Switzerland

^f Department of Natural Sciences, Middlesex University, London, UK

^g Department of Clinical Neurophysiology, UCL Hospitals, London, UK

^h Centre for Medical Image Computing, UCL, London, UK

ARTICLE INFO

Article history:

Received 23 January 2008

Revised 26 June 2008

Accepted 16 July 2008

Available online 23 July 2008

Keywords:

EIT

Anisotropy

Brain function

ABSTRACT

Electrical Impedance Tomography (EIT) is an imaging method which enables a volume conductivity map of a subject to be produced from multiple impedance measurements. It has the potential to become a portable non-invasive imaging technique of particular use in imaging brain function. Accurate numerical forward models may be used to improve image reconstruction but, until now, have employed an assumption of isotropic tissue conductivity. This may be expected to introduce inaccuracy, as body tissues, especially those such as white matter and the skull in head imaging, are highly anisotropic. The purpose of this study was, for the first time, to develop a method for incorporating anisotropy in a forward numerical model for EIT of the head and assess the resulting improvement in image quality in the case of linear reconstruction of one example of the human head. A realistic Finite Element Model (FEM) of an adult human head with segments for the scalp, skull, CSF, and brain was produced from a structural MRI. Anisotropy of the brain was estimated from a diffusion tensor-MRI of the same subject and anisotropy of the skull was approximated from the structural information. A method for incorporation of anisotropy in the forward model and its use in image reconstruction was produced. The improvement in reconstructed image quality was assessed in computer simulation by producing forward data, and then linear reconstruction using a sensitivity matrix approach. The mean boundary data difference between anisotropic and isotropic forward models for a reference conductivity was 50%. Use of the correct anisotropic FEM in image reconstruction, as opposed to an isotropic one, corrected an error of 24 mm in imaging a 10% conductivity decrease located in the hippocampus, improved localisation for conductivity changes deep in the brain and due to epilepsy by 4–17 mm, and, overall, led to a substantial improvement on image quality. This suggests that incorporation of anisotropy in numerical models used for image reconstruction is likely to improve EIT image quality.

© 2008 Elsevier Inc. All rights reserved.

Introduction

Electrical Impedance Tomography is a relatively new medical imaging method with which reconstructed tomographic images of the internal electrical impedance of a subject may be made with rings of ECG type electrodes. Its advantages are that it is fast, safe, non-invasive, low-cost and has a high temporal resolution. It has the potential to provide a uniquely useful new imaging method in clinical or experimental

neuroscience, for imaging in acute stroke (Romsauerova et al., 2006), localising the seizure onset zone in epileptics undergoing pre-operative assessment for neurosurgery (Fabrizi et al., 2006b), imaging blood volume related changes related to evoked physiological activity (Tidswell et al., 2001) or imaging fast neuronal depolarization (Gilad et al., 2005). Its principal limitation is a relatively poor image resolution and one important limiting factor is the accuracy with which brain electrical conductivity is modelled in forward models used for image reconstruction. So far most of these models have approximated body tissues as isotropic. For many body tissues in the thorax and abdomen, this appears to be a reasonable approximation. However, for imaging brain function in the adult head, this could introduce a significant

* Corresponding author. Department of Medical Physics, Malet Place Engineering Building, 2nd floor, Gower Street, London WC1E 6BT, UK.
E-mail address: juanabascal78@gmail.com (J.-F.P.J. Abascal).

inaccuracy as white matter, muscle in the scalp and brain tissue are well documented to be highly anisotropic. In EEG/MEG inverse modelling and TMS simulation studies, it has been shown that anisotropic conductivity of the skull and white matter can have a considerable impact on the electrical voltage distribution and image reconstruction (Wolters et al., 2006; De Lucia et al., 2007). A combination of MRI and EIT, MR-EIT, in which one injects electrical current using EIT and measures the magnetic flux density with MRI, has taken the first steps to provide numerical anisotropic conductivity images (Seo et al., 2004; Degirmenci and Eyuboglu, 2007), but the currently required current level to achieve a good resolution is excessively high for being safely used in the head (Liu et al., 2007). The purpose of this work was to develop a method for incorporation of anisotropy into the forward Finite Element Model used in image reconstruction, and evaluate the advantages of its use in computer simulation of EIT imaging in the human head.

The aim of EIT is to recover the conductivity inside an object by injecting electrical current and measuring voltage on the boundary (Barber and Brown, 1984; Holder, 2005). Small and safe currents are applied across a pair or several electrodes and the resulting voltage is recorded across other electrodes. Measurements from multiple electrode combinations are recorded, usually serially, which provides a set of few hundred independent voltage measurements that are non-linearly related to the conductivity of the object. EIT has been successfully employed for imaging in the thorax or abdomen, such as to image gastric emptying (Mangall et al., 1987), gastric acid secretion, and lung ventilation (Metherall et al., 1996; Harris et al., 1988). For imaging brain function, the problem is made more difficult by the presence of the skull which has a high resistance and so tends to divert current away from the brain. Studies over two decades have indicated that imaging is accurate during epilepsy and evoked activity with cortical electrodes in experimental animals, and also in realistic tank studies. In clinical studies with non-invasive scalp electrodes, there have been some encouraging findings in raw impedance data but it has not yet been possible to produce images that are sufficiently accurate for clinical or scientific routine use (see Holder, 2005 for a review). This limitation is being addressed by improvements in instrumentation (McEwan et al., 2006), signal processing (Abascal, 2007, Chapter 6) (Fabrizi et al., 2007), and image reconstruction (Abascal, 2007, Chapter 5); this work forms part of these developments.

In image reconstruction, the aim is to map boundary voltages into a 3D conductivity image. A forward model is employed to calculate boundary potentials for a given internal conductivity distribution estimate and known injected currents (Cheney et al., 1999; Lionheart, 2004). This is achieved by solving the generalised Laplace's equation with boundary conditions for the injected currents. This may include modelling of the potential drop across electrodes, such as the Complete Electrode Model (CEM) (Isaacson et al., 1990; Paulson et al., 1992). For complex geometries like the human head, for which an analytical solution does not exist, this is commonly solved numerically with the Finite Element Method (FEM). This usually employs conductivity values with an assumption of isotropy (Braess, 1997; Bagshaw et al., 2003). To our knowledge, no model which incorporates anisotropy has been reported for EIT, but it has been employed for EEG inverse source modelling (Wolters et al., 2006). A realistic finite element mesh comprising a four-shell model — scalp, skull, cerebrospinal fluid (CSF), and brain has been used for EIT of brain function (Bagshaw et al., 2003), obtained by manual segmentation and meshing from a structural imaging technique like MRI or CT (Bayford et al., 2001; Tizzard et al., 2005). A more advanced and automated methodology has been used in this work (Shindmes et al., 2007b, 2007a).

The inverse conductivity problem has a unique solution for isotropic media, from full knowledge of the complete Neumann to Dirichlet map, for piecewise analytical conductivities with smooth boundary (Kohn and Vogelius, 1984, 1985) and for continuously

differentiable conductivities in the domain (Sylvester and Uhlmann, 1987), in which the conductivity can be represented by a scalar function; but it is non-unique for anisotropic media (Lassas et al., 2003), in which the conductivity is given by a rank-2 symmetric tensor. However, it has been shown that uniqueness can be recovered by providing additional information (Lionheart, 1997; Alessandrini and Gaburro, 2001). Almost all previous EIT studies have assumed isotropic media; anisotropic conductivity was reconstructed under specific assumptions or simplistic symmetries in some exceptions (Glidewell and Ng, 1995, 1997; Pain et al., 2003; Heino et al., 2005). An empirical study of the convergence of a numerical finite element solution towards an analytical solution has been undertaken (Abascal et al., 2007). Because the forward problem is a nonlinear function of the conductivity, absolute imaging is demanding and is usually solved using iterative methods that minimise the difference between the measured and predicted data along with a regularisation functional which allows imposition of a-priori information into the solution (Arridge, 1999). In addition to nonlinearity, the reconstruction problem suffers from ill-posedness such that boundary data is more sensitive to modelling parameters than to internal conductivity (Horesh et al., 2005; Kolehmainen et al., 1997). Thus, it is unlikely that meaningful nonlinear reconstruction can be successfully achieved, where one is interested in absolute conductivity, without an accurate knowledge of modelling parameters (Lionheart, 2004). Parameters that might be expected to influence the reconstruction are the geometry, contact impedance, electrode position, and anisotropy. Because the inverse problem is ill-posed and data is usually incomplete, regularisation is required to convert the problem into a well-conditioned one.

Normalised difference data and linear reconstruction methods can reduce the influence of mismodelling (Holder, 1993, Chapter 4) (Barber and Brown, 1988), and have been hitherto considered the sole clinical remedy when a reference voltage is available (Barber and Seagar, 1987; Bagshaw et al., 2003). That is, a linear inversion method can be used to reconstruct a local change of conductivity in the brain from a small change of voltage on the scalp (Bagshaw et al., 2003). A methodology to obtain an optimum solution using Tikhonov–Phillips for the linear inversion and the Generalised Cross Validation for selecting the regularisation parameter has been proposed for EIT of brain function (Abascal, 2007, Chapter 5).

In the head, two tissues are known to have a high degree of anisotropy, white matter and skull. The conductivity ratio of normal: parallel to white matter fibres has been estimated to be 1:9 (Nicholson, 1965). The skull, which comprises two plates of cortical bone tissue enclosing the diploe, which contains marrow and blood, and so of higher conductivity, could be represented as a layer with an effective anisotropic conductivity ratio radial:tangential to the skull surface of 1:10 (Rush and Driscoll, 1968). This ratio has been adopted as an upper bound ratio for studying the influence of anisotropy of the skull for EEG (Wolters et al., 2006). In vivo, the brain conductivity tensor can be estimated from the water self-diffusion tensor by using the cross-property relation (Tuch et al., 2001; Tuch, 2002), which relates the transport model for the two tensors with the underlying microstructure. A statistical analysis of the microstructure in terms of the intra- and extra-cellular space transport coefficients yields the conductivity and diffusion tensors sharing eigenvectors. Furthermore, at quasistatic frequencies where a relatively small portion of the current flows through the intracellular space, there is a strong linear relationship between the diffusion and conductivity tensor eigenvalues. The scalp, which contains muscle, may be estimated as being 1.5 times more resistive in the radial than in the tangential direction at 50 kHz (Horesh, 2006). A comprehensive review of dielectric properties of the head tissues can be found in Horesh (2006, Chapter 2). The effect of anisotropy of muscle tissue on absolute reconstruction for EIT of the heart has been studied by providing information about the tissue boundaries, obtained from MRI, and the anisotropic structure of

muscle, which was assumed to have cylindrical symmetry and a conductivity ratio tangential:normal to the muscle of 4.3:1, in 2D and 3D (Glidewell and Ng, 1995, 1997). The anisotropy of the myocardium was not modelled because of the difficulty in estimating its anisotropic structure. In 3D, anisotropy of the muscle resulted in a shunting effect of the currents which influenced the measurements and reconstructed conductivity, however, this effect did not predominate over other modelling inaccuracies. The conductivity values tangential and normal to the muscle were reconstructed assuming that the conductivity was constant for each tissue.

So far, the influence of anisotropy for EIT of the head has not been studied, as it has been done for EEG and TMS. A high resolution FEM model was used to analyse the influence of anisotropy of white matter on the EEG forward model, incorporating the brain conductivity tensors from DT-MRI. From the results on the forward problem, it was concluded that the magnitude of the sources would be more affected than localisation, and the effect would be greater for deeper sources in the brain (Hauelsen et al., 2002). In contradiction with the previous result, a study using a 2D EEG forward model emphasized that examination of the correlation was not enough and found a high correlation yet more than 30% discrepancy in the relative potential error between the isotropic and anisotropic models. It was concluded that anisotropy of white matter would influence source localisation, as in a previous analysis, for which mismodelling using a three-shell spherical model yielded 5–10% relative error and an averaged 1.97 cm localisation error (Kim et al., 2003). A study that modelled anisotropy of the skull and white matter for the EEG forward problem analysed the effect of anisotropy by increasing the conductivity ratio of both tissues from one to ten, in terms of the Relative Difference Measure (RDM), which was described as a measure of the topographic error that compared the isotropic and anisotropic electrical fields (Wolters et al., 2006). For sources near the cortex, RDM was 11%, and was mainly affected by the skull anisotropy; for sources deeper in the brain, RDM was 10%, in which case white matter anisotropy appeared most relevant. The inverse source localisation problem has a unique inverse solution under certain constraints or priors (Pascual-Marqui, 2002; Trujillo-Barreto et al., 2004). The effect of anisotropy on the EEG inverse problem has been quantified using numerical data. Neglecting anisotropy in EEG source localisation yielded a localisation error of up to 18 mm, for superficial and 6 mm for deeper sources (Wolters, 2003, Chapter 7).

The purpose of this study has been to present a method for use of anisotropy in the forward model for EIT and to study the influence of its incorporation on the forward and inverse linear solutions in a realistic numerical head model. This included four tissue types: scalp, skull, CSF, and brain (Tizzard et al., 2005), and anisotropy was included for all except for CSF. The forward solution was analysed in terms of i) the current density norm, ii) the percentage error on the boundary voltages when anisotropy was neglected, and iii) the percentage difference between boundary voltages corresponding to a model with and without a conductivity perturbation in the brain. For the linear inverse solution, the objective was to study if use of an anisotropic forward model in image reconstruction conferred a significant benefit: images were reconstructed from simulated data produced with an anisotropic forward model. These were reconstructed with an isotropic or anisotropic model; the latter conveyed the assumption that conductivity tensors were only allowed to be modified by a scalar multiplying the tensor.

A realistic FEM model of the head incorporated segments for scalp, skull, CSF, and brain was created from the segmentation of a T1-MRI and tessellation in tetrahedra for the volume enclosed by the segmented surfaces (Shindmes et al., 2007b). Before meshing, the T1-MRI was coregistered to the reference of the DT-MRI (Friston et al., 1995; Ashburner et al., 1997). The selected isotropic conductivity values, obtained from (Horesh, 2006), corresponded to a frequency of 50 kHz that provided the largest SNR in measuring conductivity

change for epilepsy (Fabrizi et al., 2006a). Three tissues were modelled as anisotropic: the scalp, the skull, and white matter. The anisotropic information for the brain was obtained in three steps. First, for a DT-MRI, of the same subject as the T1-MRI, the diffusion tensor coefficients were interpolated at the centre of the brain tetrahedra. Second, the conductivity tensor was linearly related to the diffusion tensor by assuming both tensors shared eigenvectors and eigenvalues were linearly related. Third, the conductivity tensor trace was scaled to match the equivalent isotropic trace. The anisotropy for the scalp and skull was approximated by using the eigenvalue decomposition such that eigenvectors were two unit vectors parallel to the surface and one perpendicular to it. Eigenvalue tangential:normal ratios were 1.5:1 for the scalp (Horesh et al., 2005) and 10:1 for the skull (Wolters et al., 2006). Also, the skull and scalp tensor trace was constrained to be equal to the equivalent isotropic trace. The effect of neglecting anisotropy in the reconstructed images was studied by simulating boundary voltages which resulted from 15 perturbations in the brain. Changes in the occipital part of the brain simulated stimulation of the visual cortex, and changes in the temporal and hippocampus simulated changes in epilepsy (Fabrizi et al., 2006a). Another two perturbations were placed in the parietal and temporal lobe surrounded by white matter.

Methods

Head model: geometry and mesh

MRI and DT-MRI data sets

A T1-weighted MRI and a diffusion weighted MRI of the same subject, a 24 year old male, were obtained from the IXI-server (Rowland et al., 2004), a project that uses GRID technology for image database and image processing. Both were acquired at 3T. The DTI had 15 diffusion weighted images in different directions ($b=1000 \text{ s/mm}^2$) and a reference image B_0 ($b=0$); each of them comprised of $135 \times 135 \times 75$ voxels of resolution $1.75 \times 1.75 \times 2 \text{ mm}$. The T1 images were undersampled by half, and the inferior anterior part of the head including the mandible and nasopharynx was neglected in order to reduce the mesh size (Tizzard et al., 2005). This yielded an image of $128 \times 128 \times 75$ voxels of resolution $1.28 \times 1.28 \times 2.4 \text{ mm}$.

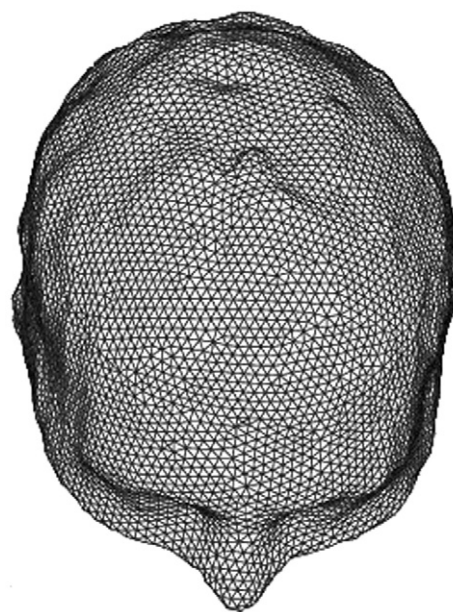


Fig. 1. Head mesh of 311,727 tetrahedra obtained by segmentation and tessellation in tetrahedra of the coregistered T1-MRI.

Coregistration of the T1 to the DTI reference

The MRI was normalised and coregistered to the B_0 and resliced after coregistration, using SPM2 (<http://www.fil.ion.ucl.ac.uk/spm/>) (Friston et al., 1995; Ashburner et al., 1997). In this process, an affine transformation followed by a nonlinear deformation was applied in order to minimise a least squares functional based on maximum entropy.

Segmentation and meshing

The coregistered T1 was segmented and tessellated to a tetrahedral FEM mesh. The segmentation and surface extraction of brain, CSF, scalp, and skull, was undertaken using BrainSuite (Shattuck and Leahy, 2002; Dogdas et al., 2002), and the meshing using Cubit (Sandia National Labs, USA) (Fig. 1) (Shindmes et al., 2007b, 2007a). The mesh contained 311,727 tetrahedra for the entire meshed head and 132,272 for the brain.

Head model: conductivity tensor estimate

Diffusion tensor estimation

Let DWI be the diffusion weighted images acquired in fifteen different directions, where g indicates the diffusion direction, the diffusion tensor D can be approximated by

$$DWI = B_0 e^{-bg^T D g} \tag{1}$$

The diffusion tensor was reconstructed using least squares minimisation over the logarithmic version of Eq. (1) (Batchelor et al., 2003).

Brain conductivity tensor

The DT coefficients D_{ij} , for $i, j = 1, 2, 3$ and $j < i$, defined in the regular grid of the MRI voxels, were interpolated, using B-splines, at the centre of the brain tetrahedra. The Fractional Anisotropy (FA) (Fig. 2) was computed for visualisation of anisotropy of white matter, from the eigenvalues $\lambda_1, \lambda_2, \lambda_3$ of D , as

$$FA = \sqrt{\frac{3}{2} \left(\frac{(\lambda_1 - \bar{\lambda})^2 + (\lambda_2 - \bar{\lambda})^2 + (\lambda_3 - \bar{\lambda})^2}{\lambda_1^2 + \lambda_2^2 + \lambda_3^2} \right)^{\frac{1}{2}}} \tag{2}$$

where $\bar{\lambda}$ is the mean of the tensor eigenvalues or mean diffusivity ($\text{trace}(D)/3$). Because the linear relation is not yet well defined within the same tissue, then the trace of the conductivity tensor was scaled to be the same as that of the equivalent isotropic trace (Kim et al., 2003) – three times the isotropic conductivity value; that is, having estimated the diffusion tensor D (1) and given the scalar isotropic conductivity σ^{iso} , the tensor σ was scaled as

$$\sigma \leftarrow \frac{3\sigma^{\text{iso}}}{\text{trace}(D)} D \tag{3}$$

Hence, both the eigenvector and eigenvalue ratios estimated from the DT were used, yet the trace was constrained to the isotropic trace $3\sigma^{\text{iso}}$.

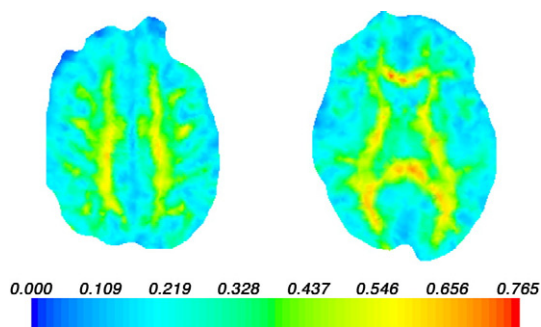


Fig. 2. Two axial sections of fractional anisotropy of the conductivity tensor in the brain.

Table 1

Isotropic value σ^{iso} and tangential:normal conductivity ratio, such that $\text{trace}(\sigma) = 3\sigma^{\text{iso}}$, for the different tissue types

Tissue	$\sigma^{\text{iso}} \text{Sm}^{-1}$	tg:normal
Grey matter	0.30	DTI
White matter	0.30	DTI
Skull	0.039	10:1
Scalp	0.44	1.5:1
CSF	1.79	1:1

Skull and scalp conductivity tensors

The skull conductivity tensor σ was approximated as $\sigma = \mathbf{V} \mathbf{S} \mathbf{V}^T$, where \mathbf{S} is a diagonal matrix of eigenvalues, which can be also interpreted as the conductivity tensor in local coordinates, and \mathbf{V} is a matrix whose columns are the eigenvectors, or a linear transformation from the local to the global coordinates. Given $\mathbf{V} = [v_1, v_2, v_3]$, v_1 and v_2 spanned a tangential plane and v_3 a normal direction to the skull surface. This defined the eigenvectors for the skull surface; the eigenvectors for the skull volume were defined by assigning each tetrahedron with the same \mathbf{V} as that of its closest surface element.

Eigenvalues corresponding to the two tangential directions and the normal direction, $\mathbf{S} = \text{diag}(s_1, s_2, s_3) = \text{diag}(s_{\text{tg}}, s_{\text{tg}}, s_{\perp})$, were computed by assigning a tangential:normal ratio of 10:1 to the skull surface and by rescaling the trace to the value of the isotropic trace, $\text{trace}(\sigma) = 3\sigma^{\text{iso}}$, then

$$\mathbf{S} = \text{diag}(0.0557, 0.0557, 0.00557) \tag{4}$$

The ratio considered here is an upper bound which has been previously considered for studying the influence of skull anisotropy for EEG (Rush and Driscoll, 1968; Wolters et al., 2006).

The anisotropy of the scalp, whose tensor was computed as in the case of the skull, had a ratio tangential:normal to the scalp surface of 1.5:1 that was approximated from its different tissues and contemplated anisotropy of muscle tissue at 50 kHz (Horesh, 2006).

Conductivity values for the head model

The conductivity tensor trace for all tissue types was constrained to match the isotropic one, that is, $\text{trace}(\sigma) = 3\sigma^{\text{iso}}$. The anisotropic conductivity tensor has been described; the isotropic tissue CSF was defined as $\sigma = \sigma^{\text{iso}} \text{diag}(1, 1, 1)$. Isotropic conductivity values and anisotropic conductivity ratios are given in Table 1. The isotropic conductivity values used were selected from (Horesh, 2006) corresponding to 50 kHz (Fig. 3).

Forward solution

The voltage was calculated using a modified version (Horesh et al., 2006) (Horesh, 2006, Chapter 4) of EIDORS 3D (Polydorides and Lionheart, 2002), piecewise linear for the voltages and constant for the conductivity, that modelled anisotropic media (Abascal and Lionheart, 2004; Abascal et al., 2007) and solved the electrical voltage for the complete electrode model equations (Paulson et al., 1992). We used a

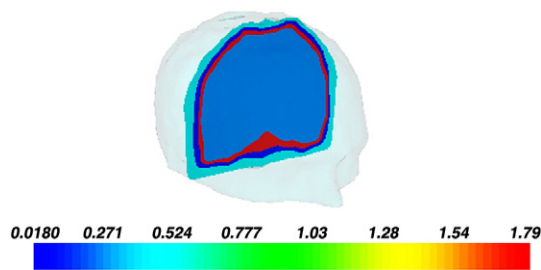


Fig. 3. Conductivity map of the isotropic head model with isotropic conductivity values (S/m): brain 0.30, CSF 1.79, skull 0.018, scalp 0.44.

Table 2
Percentage current density norm at each shell (11) for both the isotropic (ISO) and anisotropic (ANI) models

Model	Scalp	Skull	CSF	Brain
ISO	42.8	3.9	31.3	22
ANI	64.4	4	18.2	13.4
ANI/ISO	1.5	1	0.6	0.6

31-electrode position and protocol (Bayford et al., 1996), and electrode contact impedance set to 1 kΩ that simulated skin and electrode impedance (McEwan et al., 2006). The injected current was set to 5 mA.

Numerical phantom data

Relative difference data were simulated as

$$\frac{V_{inh}-V_{ref}}{V_{ref}} \quad (5)$$

where $V_{inh}=F(\sigma_{inh})$ was the boundary voltage for a conductivity distribution σ_{inh} with a perturbation in the brain, and $V_{ref}=F(\sigma_{ref})$ was the boundary voltage for a reference conductivity distribution σ_{ref} . Fifteen boundary data sets were simulated, differing in location, size, shape, and in magnitude of the conductivity change (Table 3). Two of the simulated conductivity changes resembled changes during epileptic seizures in the lateral or mesial temporal lobes (Fabrizi et al., 2006a): cylinders with a 10% conductivity decrease, 25 mm in radius and 10 mm in height, 18 cm³ in volume, in the temporal lobe, or 30 mm in length and 5.5 mm in radius, 2.5 cm³ in the hippocampus. The remaining changes were spherical changes with conductivity increase of 1% or 10% with diameters of 17 or 35 mm and were located in the occipital (7), or parietal (2) lobes or hippocampus (2).

A change in conductivity was simulated by multiplying the tensor σ by a scalar $\beta > 1$ for an increase in conductivity and $\beta < 1$ for a decrease in conductivity. Hence, it was assumed that the tensor structure did not change where simulated conductivity changes were placed in the grey matter.

Inverse solution

Scalar conductivity reconstruction of relative difference data, simulated with both the isotropic and anisotropic model, was solved by using Tikhonov inversion while GCV was employed for regularisation parameter selection for a range of twenty regularisation parameters (Abascal, 2007, Chapter 5), where reconstruction was constrained to the brain. In the isotropic case, the conductivity of the k th-finite element Ω_k was represented as $\sigma^k = \beta^k \text{diag}(1, 1, 1)$, where β^k is a multiple scalar to the unit matrix. A change of conductivity that leaves the conductivity isotropic, $\delta\sigma = \delta\beta \text{diag}(1, 1, 1)$, yields a change of voltage δV which can be represented by the linear relation (Polydorides and Lionheart, 2002)

$$\delta V = - \int_{\Omega_k} \delta\beta (\nabla u)^T \nabla u^* \quad (6)$$

where u is the electrical voltage and u^* is the voltage solved by considering the measurement electrodes as current injecting electrodes (adjoint forward solution), and for simplicity, we have assumed unit current (Polydorides and Lionheart, 2002). Let V be one of the measurements on the scalp electrodes, then the Jacobian row J^k , for $k=1, \dots, n$, where n is the number of elements, that relates that measurement to the element Ω_k is given by

$$J^k = \frac{\delta V}{\delta \beta} = - \int_{\Omega_k} (\nabla u)^T \nabla u^* = - \int_{\Omega_k} \sum_{i=1}^3 (\nabla u)_i (\nabla u^*)_i \quad (7)$$

In the universal anisotropic case, σ is a general tensor, yet, here, only a perturbation of the tensor that maintains the eigenvectors and

eigenvalue ratios affixed was considered. Let β be a multiple scalar to the tensor, such that $\sigma = \beta \sigma_0$, where σ_0 is a known tensor with $\det(\sigma_0) = 1$. Similarly to the isotropic relation (Eq. (7)), a change of conductivity, $\delta\sigma = (\delta\beta)\sigma_0$, was related to a change of voltage δV as

$$\delta V = - \int_{\Omega_k} \delta\beta (\nabla u)^T \sigma_0 \nabla u^* \quad (8)$$

Hence, the Jacobian entry J^k that relates the measurement V to the element Ω_k is given by

$$J^k = \frac{\delta V}{\delta \beta} = - \int_{\Omega_k} \sum_{i=1}^3 \sum_{j=1}^3 (\nabla u)_i (\sigma_0)_{ij} (\nabla u^*)_j \quad (9)$$

In fact, by assigning $\sigma_0 = \text{diag}(1,1,1)$, one recovers the isotropic case. The anisotropic Jacobian differs from the isotropic one, not only in the tensor product of the electrical fields given by σ_0 , but also in the fields given by the gradients of the voltages u and u^* obtained by solving the forward problem for an anisotropic conductivity reference σ_{ref} . Previous to the inversion of the Jacobian, it was row normalised to compensate for the use of relative data by its multiplication by a diagonal matrix $\text{diag}(F(\sigma_{ref})^{-1})$, where $F(\sigma_{ref})$ is the model reference voltage for a reference conductivity σ_{ref} . This step was undertaken to adjust for the fact that a relative voltage difference was provided, rather than plain voltage difference.

Comparison of the forward solutions

The isotropic and anisotropic models with the conductivity parameters from Table 2 were compared in terms of the current density norm, the percentage voltage error at the boundary by neglecting anisotropy, and the relative difference between the voltages for the reference conductivity and the perturbed conductivity, for both the isotropic and anisotropic models. A comparison of the current distribution was analysed by the current density norm

$$\|\mathcal{J}\|_2 = \|\sigma \nabla u\|_2 \quad (10)$$

Maps of current density norm were visualised for a qualitative comparison, for one current injection (Fig. 4). The total quantity of current density on each shell was employed to measure the reduction of current flowing into the brain – in order to assess the shunting effect of anisotropy, which is a relevant factor for modelling studies. The percentage current density norm at each shell was calculated as

$$100 \frac{\sum_{i \in \text{shell}} \|\mathcal{J}_i\|_2}{\sum_{i \in \text{head}} \|\mathcal{J}_i\|_2} \quad (11)$$

where i corresponded to the tetrahedral elements.

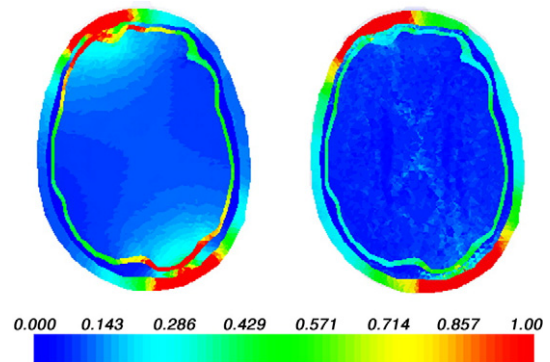


Fig. 4. Current density norm (10) cross section for the isotropic (left) and anisotropic (right) head models.

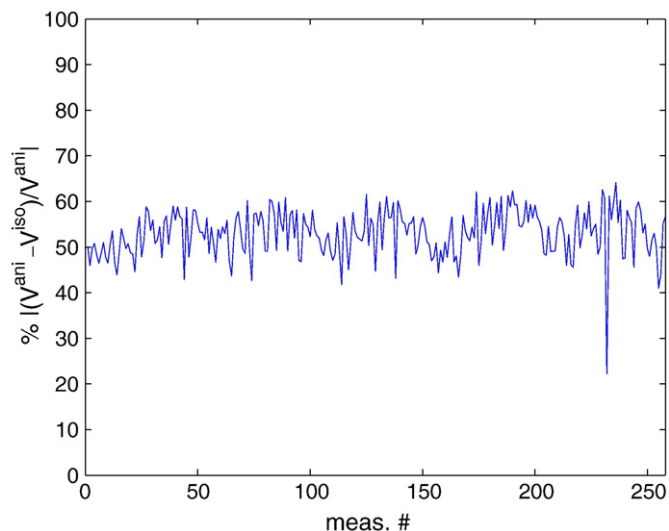


Fig. 5. Measurement voltage percentage error produced by considering the isotropic instead of the anisotropic model versus the measurement number (meas. #).

Percentage relative difference (RD) between the anisotropic and isotropic boundary voltages, for a conductivity reference, which was computed for the i th-measurement as

$$RD = 100 \frac{|F_i(\sigma_{ref}^{ani}) - F_i(\sigma_{ref}^{iso})|}{|F_i(\sigma_{ref}^{ani})|}, \quad (12)$$

gave a measure of the error of neglecting anisotropy on the scalp voltages. RD between boundary voltages with and without a 10% spherical conductivity increase in the occipital lobe, which, for the anisotropic model, was computed as

$$RD = 100 \frac{|F_i(\sigma_{inh}^{ani}) - F_i(\sigma_{ref}^{ani})|}{|F_i(\sigma_{ref}^{ani})|}, \quad (13)$$

and similarly for the isotropic model; this provided the magnitude of the scalp voltages with respect to the local conductivity change for both the isotropic and anisotropic models.

Table 3

Summary of the linear reconstruction of difference data for the isotropic (ISO) and anisotropic (ANI) data and models, for simulated conductivity changes ($\Delta\sigma$) differing in location, magnitude, and diameter (¹diameter and high for a cylindrical shape)

Location	$\Delta\sigma$ %	Diameter (mm)	Data/model	LE (mm)	Peak %
Occipital	10	35	ISO/ISO	8	3.7
Occipital	10	35	ANI/ISO	8	0.7
Occipital	10	35	ANI/ANI	8	1.3
Occipital	10	17	ANI/ISO	9	0.1
Occipital	10	17	ANI/ANI	9	0.6
Occipital	1	35	ANI/ISO	9	0.17
Occipital	1	35	ANI/ANI	24	0.55
Temporal	-10	¹ 50,10	ANI/ISO	20	-0.6
Temporal	-10	50,10	ANI/ANI	16	-8.5
Hippocampus	-10	¹ 6,30	ANI/ISO	24	-0.13
Hippocampus	-10	6,30	ANI/ANI	7	-0.47
Parietal	10	17	ANI/ISO	² 11,25	0.15,0.16
Parietal	10	17	ANI/ANI	13	0.7
Hippocampus	10	17	ANI/ISO	12	0.14
Hippocampus	10	17	ANI/ANI	12	0.41

Comparison between the anisotropic and isotropic conductivity models was done in terms of the localisation error (LE). ²This result had two maxima. Overall, the LE was 15 ± 3 for the isotropic reconstruction and 13 ± 2 for the anisotropic reconstruction (mean \pm SE).

Comparison of the reconstructed images

Three cases were considered for linear image reconstruction: i) data simulated with the isotropic model and scalar reconstruction with the isotropic conductivity model to test the inversion and set a bound for the best possible isotropic reconstruction in this setup, ii) data simulated with the anisotropic model and scalar reconstruction assuming isotropic conductivity to quantify the error associated with neglect of anisotropy, and iii) data simulated with the anisotropic model and scalar reconstruction using an anisotropic model to assess the performance of the proposed method for recovery of a multiple scalar to a general tensor. Images were visualised using the MayaVi Data Visualizer (<http://mayavi.sourceforge.net/>) and compared in terms of localisation error

$$LE = \|r_{rec} - r\|_2 \quad (14)$$

where r was the central location of the simulated conductivity change and r_{rec} was the location of the maximum peak in the region of

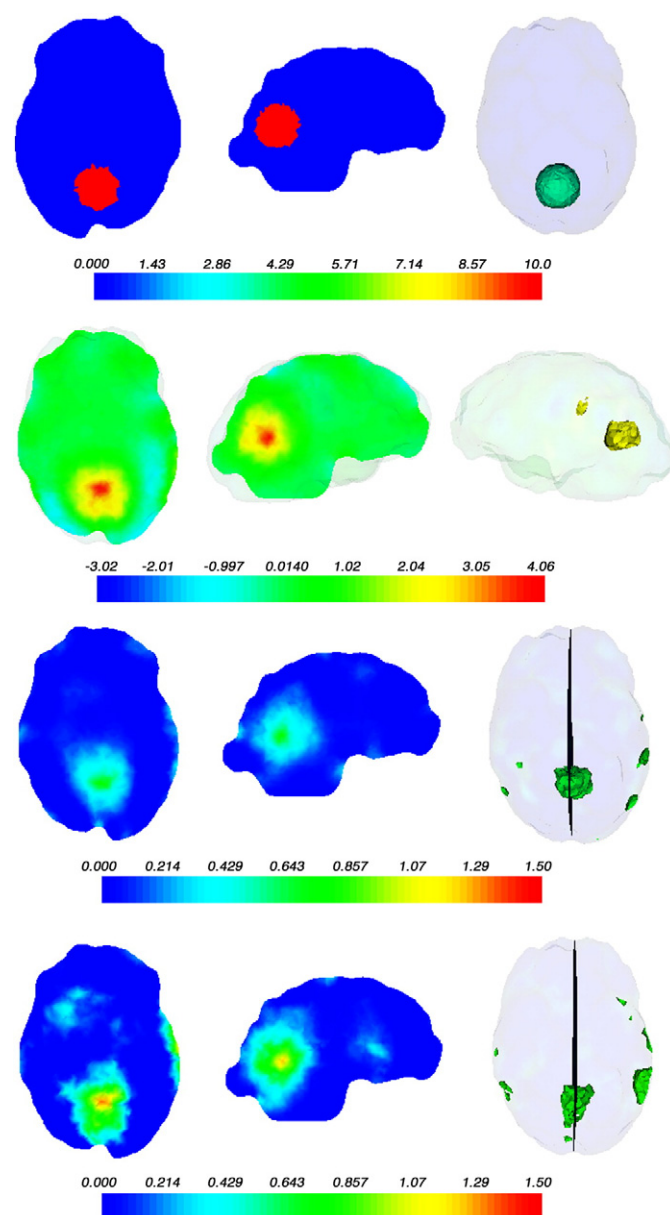


Fig. 6. Cross sections (first and second columns) and isosurface (third column) for a simulated local perturbation of 10% change and 35 mm diameter in the occipital lobe (first row), linear reconstruction of isotropic data (second row), linear reconstruction of anisotropic data with the isotropic (third row) and anisotropic (last row) model.

interest of the reconstructed image. The maximum value (peak) between the isotropic and anisotropic models was also compared. This measure decreases with the amount of regularisation imposed and so it must be treated with more caution. In addition to the LE, images of the simulated and reconstructed conductivity changes were displayed as axial and sagittal cross sections at the centre of the simulated locations and as an isosurface 3D image (a surface that represents points of a constant value) to allow identification of artefacts in the entire brain.

Results

Comparison of the forward isotropic and anisotropic solutions

In the anisotropic model, the current flowed mainly tangential to the scalp and skull surfaces with respect to the isotropic model (Fig. 4). The total current that flowed into the brain was reduced by a factor of two (Table 2). In the brain, current was uniformly distributed in the isotropic model, and flowed along the white matter fibres in the anisotropic model. Neglecting anisotropy led to an average relative voltage error at the boundary of 53% (Fig. 5). Modelling a local conductivity change of 10% in the occipital part of the brain led to a change of 0.0124% in the mean boundary voltage for the anisotropic model, and a five fold greater change of 0.061% for the isotropic model; the mean boundary voltages was five times smaller for the anisotropic model.

Effect of anisotropy on linear image reconstruction of difference data

Reconstruction of data simulated with the isotropic model

For a simulated conductivity change of 10% in the occipital lobe, the maximum reconstructed peak was 4% and the localisation error was 8 mm, which was set as a lower bound related to the ill-posedness and regularisation of the problem (first row in Table 3, Fig. 6).

Reconstruction of data simulated with the anisotropic model

Neglecting anisotropy in the reconstruction led to significant errors in the reconstructed images. In the occipital lobe, there was no significant effect on localisation. However, an increase of spurious artefacts may be seen when the diameter of the conductivity perturbation was reduced from 35 to 17 mm diameter (Fig. 6) and when the conductivity change was reduced from 10 to 1%, which simulated stimulation of the visual cortex (Fig. 6). For epilepsy related changes (Fig. 6), the localisation error was 20 mm in the temporal lobe, which may be due to shape of the simulated change, and 24 mm in the hippocampus, for which the simulated change was deep in the brain. For the other locations (Fig. 6), localisation errors were 11–13 mm and a significant decrease in image quality may be observed as artefacts of similar magnitude as the change of interest. In general, neglecting anisotropy affected image quality with the emergence of spurious artefacts outside the region of interest, mainly on the surface of the brain. Modelling anisotropy in the linear reconstruction with the proposed method led to a substantial improvement in localisation

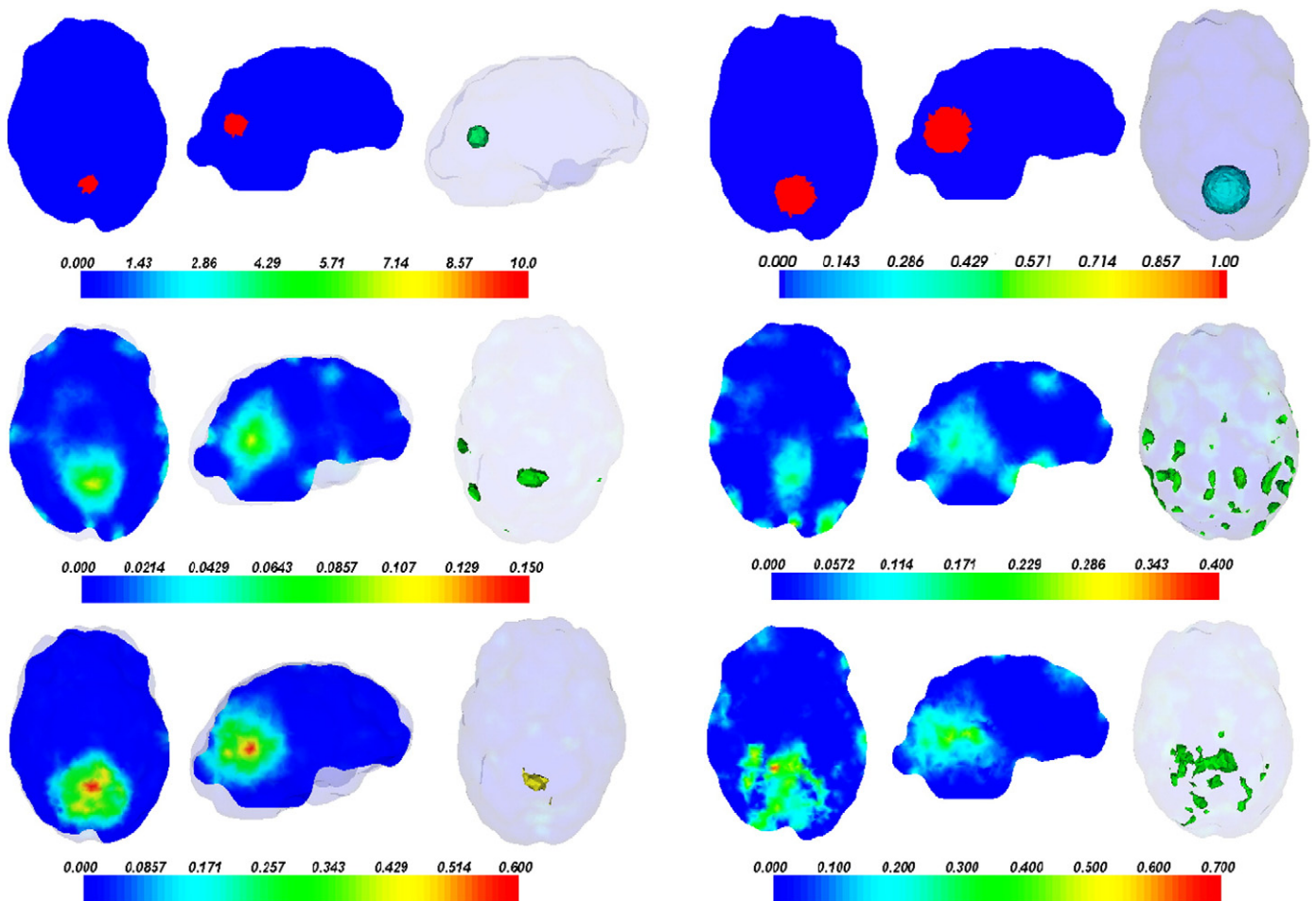


Fig. 7. Cross sections (first and second columns) and isosurface (third column) for a simulated local perturbation of 10% change and 17 mm diameter (three columns on the left) and a simulated local perturbation of 1% change and 35 mm diameter (three columns on the right) in the occipital lobe (first row), and linear reconstruction of anisotropic data with the isotropic (second row) and anisotropic (last row) model.

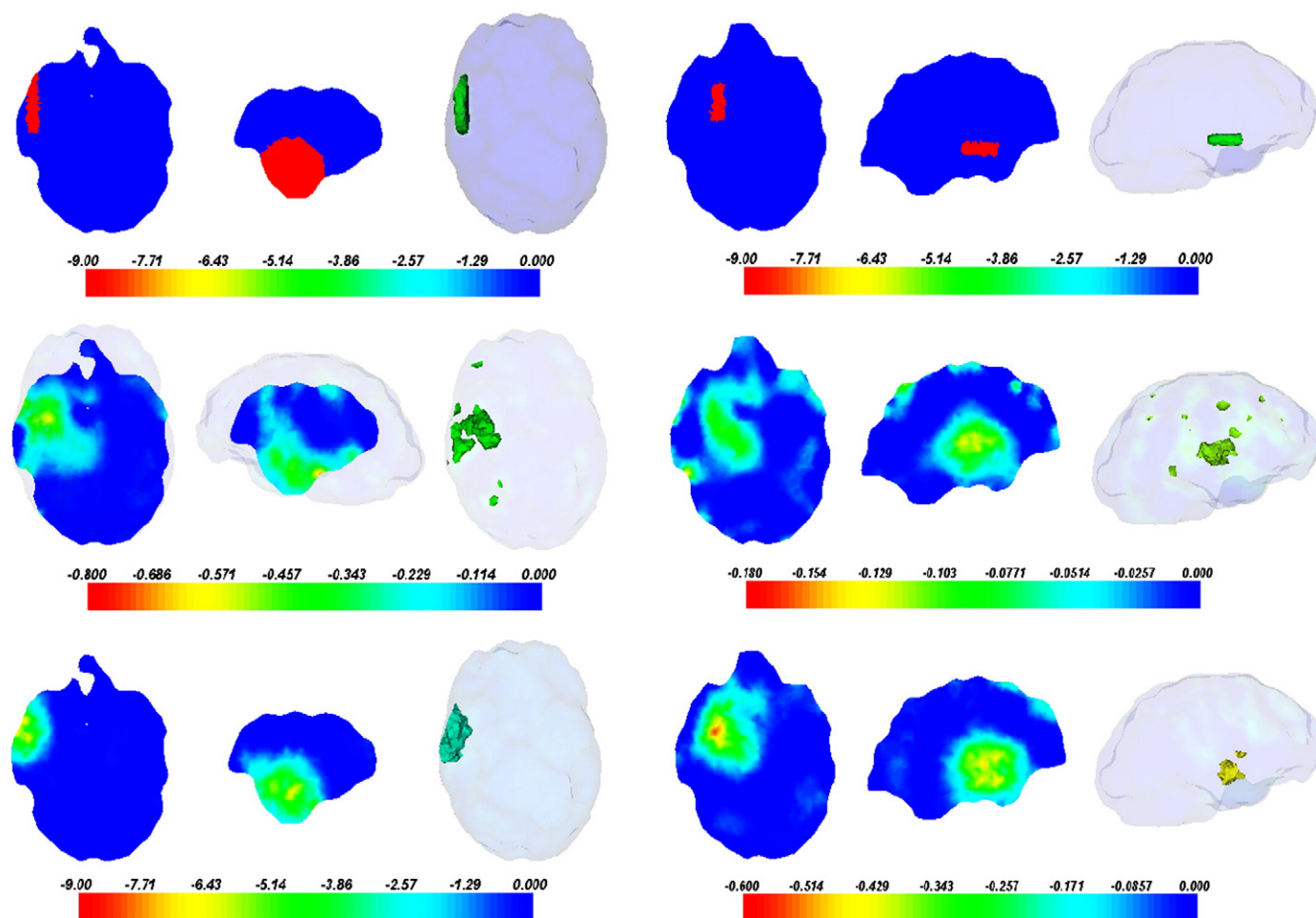


Fig. 8. Cross sections (first and second columns) and isosurface (third column) for a simulated cylindrical 10% local decrease in conductivity in the temporal lobe (three columns on the left) and in the hippocampus (three columns on the right), which resemble typical changes during temporal lobe seizures, and linear reconstruction of anisotropic data with the isotropic (second row) and anisotropic (last row) model.

error, to 8–16 mm, shape of the reconstructed conductivity change, and in image quality with reduction of spurious artefacts, except for the simulation in the visual cortex of 1% conductivity change, for which although the decrease of artefacts was significant, the localisation error was 24 mm. A decrease of image quality with both the isotropic and anisotropic models may be observed for the 1% conductivity change. The maximum peak of the reconstructed image with the anisotropic model was larger and more accurate than the corresponding isotropic reconstruction where the amplitude of the peaks decreased as structure (regularisation) was imposed more strictly; reconstruction with the anisotropic model led to improvement in image quality (Figs. 7–9).

In summary, neglecting anisotropy led to a localisation error up to 24 mm and worsened image quality while scalar linear reconstruction based on anisotropic modelling reduced localisation error and improved shape, and peak value. Overall, the LE was 15 ± 3 mm for the isotropic reconstruction and 13 ± 2 mm for the anisotropic reconstruction. For the epilepsy changes, modelling anisotropy was essential to obtain good images and reduced localisation error by about three fold; on the other hand, for visual stimulation there was not significant improvement.

Discussion

Summary of results

A preferred direction of current flow tangential to the scalp and skull surfaces and along white matter fibres was evident in the current

density map. In the brain in the anisotropic model, current flowed along fibres parallel to the injection field, avoiding grey matter and white matter fibres whose paths were perpendicular to the current flow direction. Skull anisotropy introduced a shunting effect: in a comparison of the total current density flowing through the different brain tissues, the current that flowed into the brain in the anisotropic model decreased by two fold with respect to the isotropic model, and 50% more current was found in the anisotropic scalp than in the isotropic case. Neglecting anisotropy led to errors of up to fifty percent on the boundary voltages. For a local increase of conductivity of 10% in the occipital lobe, boundary voltages were five times less in the anisotropic case. The effect of anisotropy on the linear reconstructed images was analysed in terms of the localisation error, for which a lower bound of 8 mm was set from the simulation and reconstruction of a conductivity change in the isotropic model; that is, the intrinsic error due to the ill-posedness of the problem in conjunction with the application of the chosen regularisation scheme to overcome it. Neglecting anisotropy led to a localisation error between 8 and 24 mm where high errors occurred when the simulated change was deep in the brain or surrounded by white matter; the largest error was for a change in the hippocampus. A small increase of error was found for a decrease by two fold of the diameter of the inclusion or simulation of a smaller conductivity change. The proposed scalar reconstruction based on the anisotropic model led to an improvement of the localisation error up to three fold in the hippocampus and by a lesser amount for other conductivity changes, but generally it led to errors between 8 and 24 mm. The overall error was 15 ± 3 for the isotropic

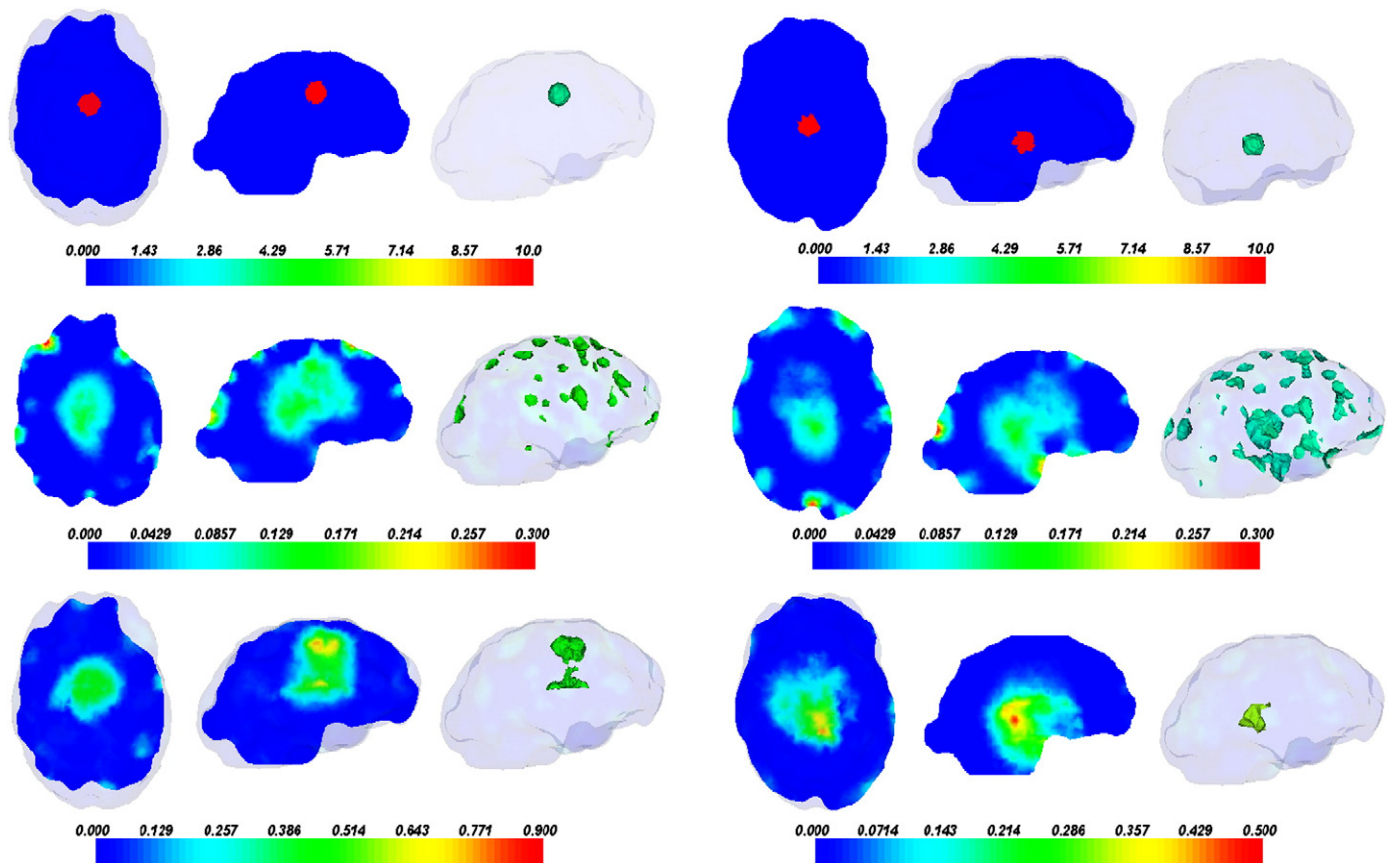


Fig. 9. Cross sections (first and second columns) and isosurface (third column) for a simulated 10% local increase in conductivity and 16 mm diameter in the parietal lobe (three columns on the left) and near the hippocampus (three columns on the right), and linear reconstruction of anisotropic data with the isotropic (second row) and anisotropic (last row) model.

reconstruction and 13 ± 2 for the anisotropic reconstruction. In terms of image quality, neglecting anisotropy led to spurious artefacts, outside the region of interest mainly on the brain surface; modelling anisotropy led to an improvement in the reconstructed shape and peak value and reduction of spurious artefacts.

Technical issues

The overall aim of this work was to estimate the effect of anisotropy for a realistic model; however, some simplifications were made. Isotropic conductivity values vary with the frequency and the conditions at which they are acquired. In addition to that, the reported values vary across the literature. The selected isotropic conductivity corresponded to published values at 50 kHz (Horesh, 2006), which yielded the largest measurable changes in epilepsy (Fabrizi et al., 2006a). White matter conductivity was determined from DT-MRI up to a scalar factor, where the conductivity and diffusion tensors are linearly related at low frequencies, that is, for frequencies no larger than 1 or 50 kHz. Then, the scalar factor was determined by constraining the anisotropic tensor to be equal to the isotropic trace at 50 kHz. A previous study has constrained the trace for the white matter tensor. The rationale of that choice was based on the principle that conductivity and diffusion tensors are linearly related across different tissue types, but this linear relation is not as strong within the same tissue (Kim et al., 2003). The scalp anisotropy was approximated, by accounting for the scalp anisotropy and tissue composition at 50 kHz, with a conductivity ratio tangential:normal to the scalp surface of 1.5:1 (Horesh, 2006), it may be larger at other frequencies. The muscle conductivity has been previously modelled with a ratio 4.3:1 (Glidewell and Ng, 1995, 1997). Here, the skull

conductivity ratio tangential:normal to the skull surface was chosen as 10:1 (Rush and Driscoll, 1968), which was the largest ratio discussed for EEG studies (Wolters et al., 2006), so it was selected as an upper bound to account for the largest effect of neglecting anisotropy. Besides, it was found that the bone conductivity on the three orthogonal directions was constant up to 10 kHz (Reddy and Saha, 1984). In conclusion, modelling different conductivity values may vary the results slightly, yet this analysis was intended to estimate the importance of anisotropy for EIT of the head.

Incorporation of anisotropy within an accurate model of the head had a significant influence on the forward model. For the inversion, the linear approximation for reconstruction of difference data was used, which reduces modelling and experimental errors. For the applications of principal interest to our group, like epilepsy and evoked responses, a reference voltage is known and few percent conductivity changes in the brain lead to a much smaller data change on the scalp, and so second order changes can be neglected. Thus, linear reconstruction of anisotropic difference data using the isotropic model was possible but had a significant effect on localisation and image quality. On the other hand, for other relevant applications such as acute stroke, a reference data is not available, and so nonlinear reconstruction of absolute conductivity is more likely to be more influenced by neglecting anisotropy. For the incorporation of anisotropy in the inversion, the tensor structure was assumed to be known – eigenvectors and eigenvalue ratios were provided, and reconstruction was of a scalar multiplying this tensor: this resembles isotropic reconstruction which has been proven to have a unique solution (Lionheart, 1997). As the tensor structure is then assumed to be known, only conductivity changes located in the grey matter can possibly be reconstructed, and changes in white matter affecting the

anisotropic structure of white matter cannot be accurately modelled. In this work, reconstruction was undertaken using the anisotropic model as for the simulation of the data. This was intended to demonstrate the influence of neglecting anisotropy on linear inversion for computer simulation; further study is needed to assess the eventual overall benefit of the incorporation of anisotropy on the inversion for in vivo data.

In general, the peak in the reconstructed images provided an estimation of the simulated conductivity changes, where location and spurious artefacts were reduced when the anisotropic model was used. The magnitude of the reconstructed images was lower than the simulated ones, as was expected from the filtering effect of regularisation of the inverse solution, and the sign was satisfactorily recovered. Again, the magnitude was better when using the anisotropic model, which may be due to the fact that less regularisation was needed. The shape of the reconstructed conductivity changes, especially for epilepsy changes, was only approximately recovered. This may be caused by several factors: larger changes in magnitude and size in epilepsy, the effect of regularisation, and incomplete sampling.

This analysis has been done using the same mesh for all models. The relevance of anisotropy cannot be then concluded till this study is extended and the effect of anisotropy is shown to be mesh independent and compared to other modelling errors.

Comparison with previous results

Previous results could be used to set a lower bound for the localisation error. Distortion of an MRI at the coregistration stage may lead to errors up to 5 mm, yet they can be reduced to 1 mm using specific methods (Maurer et al., 1996; Tizzard et al., 2005). Also, the segmentation and boundaries extraction from a T1-MRI had 1–2 mm error (Dogdas et al., 2002). A lower bound from mismodelling which would be unavoidable in practice, including factors as the inhomogeneity of the skull, for 64 electrodes and 2% noise, led to 10 mm localisation error (Ollikainen et al., 1999). An assessment of the head-shell model for EIT of brain function was undertaken on simulated, tank, and human data using linear reconstruction (Bagshaw et al., 2003). Localisation errors were (in millimeters), for simulated data from a homogeneous head-shaped model 21 ± 6 for head-shaped reconstruction and 24 ± 10 for spherical reconstruction; for homogeneous head tank data, 13 ± 7 for head-shaped reconstruction and 19 ± 8 for spherical reconstruction; and for the head with skull tank data, 26 ± 8 for head-shaped reconstruction and 24 ± 8 for spherical reconstruction. For human data, an improvement in image quality was found. It was concluded that realistic conductivity values and accurate geometry led to slight improvements where improvements in image quality were more significant than localisation error and resolution. Neglecting anisotropy of the skull and white matter in EEG modelling studies yielded an upper bound of 30% in the forward solution and 18 mm localisation error. The results presented here led to a 50% change in the forward solution, which suggests a significant influence of modelling the anisotropy of the scalp. While for epilepsy there is a reference voltage, and therefore linear reconstruction of difference data is recommended, for stroke detection, no time difference data is possible, and it appears that absolute and multi-frequency imaging are required. For absolute imaging, one would expect anisotropy to have a far more significant effect in absolute nonlinear reconstruction than for linear reconstruction of difference data. In an assessment study with absolute simulated and tank measurements, the effect of geometric errors over stroke modelling were analysed and it was found that geometric errors were by far larger than those introduced by the pathological perturbation (Horesh et al., 2005) (Horesh, 2006, Chapters 4 and 6). Linear reconstruction neglecting anisotropy led here to an error of 24 mm, which compared with the 13–26 mm error from the EIT studies on tank data, which

suggests that for linear reconstruction of conductivity changes deep in the brain, modelling anisotropy will improve results if mismodelling errors of the electrodes accounted in the EIT real studies are resolved (Bagshaw et al., 2003).

Conclusion and suggestions for further work

Modelling anisotropy therefore appears to be required to obtain an accurate forward solution and good image quality images and a low localisation error for linear reconstruction, especially if the imaged changes are deep in white matter. A more significant influence is likely to be for absolute imaging, for which we are studying the possibility of anisotropic tensor reconstruction assuming that a-priori information is available to correct for a wrong anisotropic estimation. Further work is needed to show that anisotropic modelling is mesh independent, and to compare its effect to other modelling errors. In addition to this, analysis of the influence of anisotropic structure on real phantoms would determine the relevance of anisotropy for many other EIT applications.

Appendix A. Supplementary data

Supplementary data associated with this article can be found, in the online version, at doi:10.1016/j.neuroimage.2008.07.023.

References

- Abascal, J.F.P.-J., 2007. Improvements in reconstruction algorithms for electrical impedance tomography of the head. Ph.D. thesis, University College London, London, UK.
- Abascal, J.F.P.-J., Arridge, S.R., Lionheart, W.R.B., Bayford, R.H., Holder, D.S., 2007. Validation of a finite element solution for electrical impedance tomography in an anisotropic medium. *Physiol. Meas.* 28, S129–S140.
- Abascal, J.F.P.-J., Lionheart, W.R.B., 2004. Rank analysis of the anisotropic inverse conductivity problem. *Proc. ICEBI XII-EIT V. Gdansk, Poland*, pp. 511–514.
- Alessandrini, G., Gaburro, R., 2001. Determining conductivity with special anisotropy by boundary measurements. *SIAM J. Math. Anal.* 33 (1), 153–171.
- Arridge, S.R., 1999. Optical tomography in medical imaging. *Inv. Problems* 15, R41–R93.
- Ashburner, J., Neelin, P., Collins, D.L., Friston, A.C.E.K.J., 1997. Incorporating prior knowledge into image registration. *NeuroImage* 6, 344–352.
- Bagshaw, A.P., Liston, A.D., Bayford, R.H., Tizzard, A., Gibson, A.P., Tidswell, A.T., Sparkes, M.K., Dehghani, H., Binnie, C.D., Holder, D.S., 2003. Electrical impedance tomography of human brain function using reconstruction algorithms based on the finite element method. *NeuroImage* 20, 752–764.
- Barber, D.C., Brown, B.H., 1984. Applied potential tomography. *J. Phys. E: Sci. Instrum.* 17, 723–733.
- Barber, D.C., Brown, B.H., 1988. Errors in reconstruction of resistivity images using a linear reconstruction technique. *Clin. Phys. Physiol. Meas.* 9 (Suppl. A), 101–104.
- Barber, D.C., Seagar, A.D., 1987. Fast reconstruction of resistance images. *Clin. Phys. Physiol. Meas.* 8, 47–54.
- Batchelor, P.G., Atkinson, D., Hill, D.L., Calamante, F., Connelly, A., 2003. Anisotropic noise propagation in diffusion tensor MRI sampling schemes. *Magn. Reson. Med.* 49 (6), 1143–1151.
- Bayford, R.H., Boone, K.G., Hanquan, Y., Holder, D.S., 1996. Improvement of the positional accuracy of EIT images of the head using a Lagrange multiplier reconstruction algorithm with diametric excitation. *Physiol. Meas.* 17, A49–A57.
- Bayford, R.H., Gibson, A., Tizzard, A., Tidswell, A.T., Holder, D.S., 2001. Solving the forward problem for the human head using IDEAS (Integrated Design Engineering Analysis Software) a finite element modelling tool. *Physiol. Meas.* 22, 55–63.
- Braess, D., 1997. *Finite Elements*. Cambridge University Press, Cambridge, UK.
- Cheney, M., Isaacson, D., Newell, J.C., 1999. Electrical impedance tomography. *SIAM Rev.* 41 (1), 85–101.
- De Lucia, M., Parker, G.J.M., Embleton, K., Newton, J.M., Walsh, V., 2007. Diffusion tensor MRI-based estimation of the influence of brain tissue anisotropy on the effects of transcranial magnetic stimulation. *NeuroImage* 36, 1159–1170.
- Degimenci, E., Eyuboglu, B.M., 2007. Anisotropic conductivity imaging with MREIT using equipotential projection algorithm. *Phys. Med. Biol.* 52, 7229–7242.
- Dogdas, B., Shattuck, D.W., Leahy, R.M., 2002. Segmentation of skull in 3d human MR images using mathematical morphology. *Progr. Biomed. Opt. Imaging* 3 (22), 1553–1562.
- Fabrizi, L., Horesh, L., McEwan, A., Holder, D., 2006a. A feasibility study for imaging of epileptic seizures by EIT using a realistic FEM of the head. *Proc. of 7th conference on biomedical applications of electrical impedance tomography*. Kyung Hee University and COEX, Korea, pp. 45–48.
- Fabrizi, L., Sparkes, M., Horesh, L., Abascal, J.F.P.-J., McEwan, A., Bayford, R.H., Elwes, R., Binnie, C.D., Holder, D.S., 2006b. Factors limiting the application of electrical impedance tomography for identification of regional conductivity changes using scalp electrodes during epileptic seizures in humans. *Physiol. Meas.* 27, S163–S174.

- Fabrizi, L., McEwan, A., Woo, E., Holder, D.S., 2007. Analysis of resting noise characteristics of three EIT systems in order to compare suitability for time difference imaging with scalp electrodes during epileptic seizures. *Physiol. Meas.* 28, S217–S236.
- Friston, K.J., Ashburner, J., Frith, C.D., Poline, J.-B., 1995. Spatial registration and normalization of images. *Hum. Brain Mapp.* 2, 165–189.
- Gilad, O., Horesh, L., Ahadzi, G.M., Bayford, R.H., Holder, D.S., 2005. Could synchronized neuronal activity be imaged using Low Frequency Electrical Impedance Tomography (LFEIT)? 6th Conference on Biomedical Applications of Electrical Impedance Tomography. London, UK.
- Glidewell, M., Ng, K.T., 1995. Anatomically constrained electrical-impedance tomography for anisotropic bodies via a two-step approach. *IEEE Trans. Med. Imag.* 14, 498–503.
- Glidewell, M., Ng, K.T., 1997. Anatomically constrained electrical impedance tomography for three-dimensional anisotropic bodies. *IEEE Trans. Med. Imag.* 16 (5), 572–580.
- Harris, N.D., Suggett, A.J., Barber, D.C., Brown, B.H., 1988. Applied potential tomography: a new technique for monitoring pulmonary function. *Clin. Phys. Physiol. Meas.* 9 (Suppl. A), 79–85.
- Hauelsen, J., Tuch, D.S., Ramon, C., Schimpf, P.H., Wedeen, V.J., George, J.S., Belliveau, J.W., 2002. The influence of brain tissue anisotropy on human EEG and MEG. *NeuroImage* 15 (1), 159–166.
- Heino, J., Somersalo, E., Kaipio, J.P., 2005. Compensation for geometric mismodelling by anisotropies in optical tomography. *Opt. Express* 13 (1), 296–308.
- Holder, D.S., 1993. *Clinical and Physiological Applications of EIT*. UCL Press, London, UK.
- Holder, D.S., 2005. *Electrical Impedance Tomography*. IOP, London, UK.
- Horesh, L., 2006. Some novel approaches in modelling and image reconstruction for multi-frequency electrical impedance tomography of the human brain. Ph.D. thesis, University College London, London, UK.
- Horesh, L., Gilad, O., Romsauerova, A., Arridge, S.R., Holder, D.S., 2005. Stroke type by Multi-Frequency Electrical Impedance Tomography (MFEIT)—a feasibility study. In: 6th Conference on Biomedical Applications of Electrical Impedance Tomography. UCL, London, UK.
- Horesh, L., Schweiger, M., Bollhofer, M., Douiri, A., Arridge, S.R., Holder, D.S., 2006. Multilevel preconditioning for 3d large-scale soft field medical applications modelling. information and systems sciences. *Information and Systems Sciences, Special Issue on Computational Aspect of Soft Field Tomography* 532–556.
- Isaacson, D., Newell, J., Simske, S., Goble, J., 1990. NOSER: an algorithm for solving the inverse conductivity problem. *Int. J. Imaging Syst. Technol.* 2, 66–75.
- Kim, S., Kim, T.-S., Zhou, Y., Singh, M., 2003. Influence of conductivity tensors in the finite element model of the head on the forward solution of EEG. *IEEE Trans. Nucl. Sci.* 50, 133–139.
- Kohn, R.V., Vogelius, M., 1984. Determining conductivity by boundary measurements, interior results II. *Commun. Pure Appl. Math.* 37, 281–298.
- Kohn, R.V., Vogelius, M., 1985. Determining conductivity by boundary measurements, interior results II. *Commun. Pure Appl. Math.* 38, 643–667.
- Kolehmainen, V., Vauhkonen, M., Karjalainen, P.A., Kaipio, J.P., 1997. Assessment of errors in static electrical impedance tomography with adjacent and trigonometric current patterns. *Physiol. Meas.* 18, 289–303.
- Lassas, M., Taylor, M., Uhlmann, G., 2003. The Dirichlet-to-Neumann map for complete Riemannian manifolds with boundary. *Commun. Anal. Geom.* 11, 207–221.
- Lionheart, W.R.B., 1997. Conformal uniqueness results in anisotropic electrical impedance imaging. *Inverse Problems* 13, 125–134.
- Lionheart, W.R.B., 2004. EIT reconstruction algorithms: pitfalls, challenges and recent developments. *Physiol. Meas.* 25, 125–142.
- Liu, J.J., Seo, J.K., Sini, M., Woo, E.J., 2007. On the conductivity imaging by MREIT: available resolution and noisy effect. *Inverse Problems in Applied Sciences*, Vol. 73. IOP, pp. 1742–6596.
- Mangall, Y.F., Baxter, A., Avill, R., Bird, N., Brown, B., D., B., Seager, A., Johnson, A., 1987. Applied potential tomography: a new non-invasive technique for assessing gastric function. *Clin. Phys. Physiol. Meas.* 8, 119–129.
- Maurer, C.R.J., Aboutanos, G.B., Dawant, B.M., Gadamssety, S., Margolin, R.A., Maciunas, R.J., Fitzpatrick, J.M., 1996. Effect of geometrical distortion correction in MR on image registration accuracy. *J. Comput. Assist. Tomogr.* 20 (4), 666–679.
- McEwan, A., Romsauerova, A., Yerworth, R., Horesh, L., Bayford, R., Holder, D., 2006. Design and calibration of a compact multi-frequency EIT system for acute stroke imaging. *Physiol. Meas.* 27, S199–S210.
- Metherall, P., Barber, D.C., Smallwood, R.H., Brown, B.H., 1996. Three-dimensional electrical impedance tomography. *Nature* 380, 509–512.
- Nicholson, P.W., 1965. Specific impedance of cerebral white matter. *Exp. Neurol.* 13, 386–401.
- Ollikainen, J.O., Vauhkonen, M., Karjalainen, P.A., Kaipio, J.P., 1999. Effects of local skull inhomogeneities on EEG source estimation. *Med. Eng. Phys.* 21 (3), 143–154.
- Pain, C.C., Herwanger, J.V., Saunders, J.H., Worthington, M.H., Cassiano de Oliveira, R.E., 2003. Anisotropic and the art of resistivity tomography. *Inverse Problems* 19, 1081–1111.
- Pascual-Marqui, R.D., 2002. Standardized low resolution brain electromagnetic tomography (SLORETA): technical details. *Methods Find. Exp. Clin. Pharmacol.* 24D, 5–12.
- Paulson, K., Breckon, W., Pidcock, M., 1992. Electrode modelling in electrical impedance tomography. *SIAM J. Appl. Math.* 52, 1012–1022.
- Polydorides, N., Lionheart, W.R.B., 2002. A Matlab toolkit for three-dimensional electrical impedance tomography: a contribution to the Electrical Impedance and Diffuse Optical Reconstruction Software project. *Meas. Sci. Technol.* 13, 1871–1883.
- Reddy, G.N., Saha, S., 1984. Electrical and dielectric properties of wet bone as a function of frequency. *IEEE Trans. Biomed. Eng.* 31 (3), 296–302.
- Romsauerova, A., Ewan, A.M., Horesh, L., Yerworth, R., Bayford, R.H., Holder, D.S., 2006. Multi-frequency electrical impedance tomography (EIT) of the adult human head: initial findings in brain tumours, arteriovenous malformations and chronic stroke, development of an analysis method and calibration. *Physiol. Meas.* 27 (5), S147–S161.
- Rowland, A.L., Burns, M., Hartkens, T., Hajnal, J.V., Rueckert, D., Hill, D.L.G., 2004. Information extraction from images (ixi): image processing workflows using a grid enabled image database. In *Proc of Distributed Databases and Process Medical Image Comput (DiDaMIC)*, pp. 55–64. Rennes, France.
- Rush, S., Driscoll, D., 1968. Current distribution in the brain from surface electrodes. *Anaesthesia and analgetica* 47 (6), 717–723.
- Seo, J.K., Kwon, O., Woo, E.J., 2004. Anisotropic conductivity image reconstruction problem in Bz-based MREIT. *Proc. ICEBI XII-EIT V*, pp. 531–534. Gdansk, Poland.
- Shattuck, D.W., Leahy, R.M., 2002. BrainSuite: an automated cortical surface identification tool. *Med. Image Anal.* 6 (2), 129–142.
- Shindmes, R., Horesh, L., Holder, D.S., 2007a. The effect of using patient specific finite element meshes for modelling and image reconstruction of electrical impedance tomography of the human head. In progress.
- Shindmes, R., Horesh, L., Holder, D.S., 2007b. Technical report – generation of patient specific finite element meshes of the human head for electrical impedance tomography. In progress.
- Sylvester, J., Uhlmann, G., 1987. A global uniqueness theorem for an inverse boundary value problem. *Annals of Math* 125, 153–169.
- Tidswell, T., Gibson, A., Bayford, R.H., Holder, D.S., 2001. Three-dimensional electrical impedance tomography of human brain activity. *NeuroImage* 13, 283–294.
- Tizzard, A., Horesh, L., Yerworth, R.J., Holder, D.S., Bayford, R.H., 2005. Generating accurate finite element meshes for the forward model of the human head in EIT. *Physiol. Meas.* 26, S251–S261.
- Trujillo-Barreto, N.J., Aubert-Vzquez, E., Valds-Sosa, P.A., 2004. Bayesian model averaging in EEG/MEG imaging. *NeuroImage* 21, 1300–1319.
- Tuch, D.S., 2002. Diffusion MRI of complex tissue structure. Ph.D. thesis, Massachusetts Institute of Technology, Massachusetts.
- Tuch, D.S., Wedeen, V.J., Dale, A.M., George, J.S., Belliveau, J.W., 2001. Conductivity tensor mapping of the human brain using diffusion tensor MRI. *Proc. Natl. Acad. Sci. USA* 98 (20), 11697–11701.
- Wolters, C.H., 2003. Influence of tissue conductivity inhomogeneity and anisotropy on EEG/EMG based source localization in the human brain. Ph.D. thesis, University of Leipzig, Leipzig, Germany.
- Wolters, C.H., Anwander, A., Tricoche, X., Weinstein, D., Koch, M.A., MacLeod, R.S., 2006. Influence of tissue conductivity anisotropy on EEG/EMG field and return current computation in a realistic head model: a simulation and visualization study using high-resolution finite element modeling. *NeuroImage* 30 (3), 813–826.